# $Cs^+$ incorporation into $CH_3NH_3PbI_3$ perovskite: Broad miscibility gap and stability enhancement

Ralf G. Niemann[a], Laxman Gouda[b], Jiangang Hu[b], Shay Tirosh[b], Ronen Gottesman[b], P.J. Cameron[a] and Arie Zaban[b]

## Abstract

Recent progress in the field of hybrid organic-inorganic perovskites $ABX_3$ for photovoltaics has given cells with certified efficiencies of 22.1 % solar to electric power, mainly based upon the hybrid inorganic-organic methylammonium lead iodide perovskite $MAPbI_3$ ($MA^+ = CH_3NH_3^+$). Up to now, one of the biggest drawbacks is poor stability towards humidity and temperature. A substitution of the organic $MA^+$ with inorganic $Cs^+$ yields the extremely stable structure $CsPbI_3$, which however forms a yellow $\delta$-phase at room-temperature that is not photoactive. In this study we have systematically explored the mixed cation perovskite $Cs_xMA_{1-x}PbI_3$ as a material and demonstrate its benefits for photovoltaic applications. We exchanged the A-side cation by dipping $MAPbI_3$ films into a CsI solution, thereby incrementally replacing the $MA^+$ in a time-resolved dipping process and analysed the resulting thin-films with UV-Vis, XRD, EDAX, SEM and optical depth-analysis in a high-throughput fashion. Additional in-situ measurements of UV-Vis and XRD allowed us to look at the kinetics of the formation process. The results showed a discontinuity during the conversion. Firstly, small amounts of $Cs^+$ are incorporated into the structure. After a few minutes, the Cs content approaches a limit and the material converts into the pure $\delta$-$CsPbI_3$, indicating a broad miscibility gap. We compared this cation exchange to a one-step crystallisation approach and found the same respective effect of phase segregation, indicating that the miscibility gap is an intrinsic feature rather than a kinetic effect. Optical and structural properties changed continuously for small Cs incorporations and become unsteady due to phase segregation for larger Cs contents. We estimate the miscibility gap of $Cs_xMA_{1-x}PbI_3$ to start at a Cs ratio $x = 0.13$, based on combined measurements of EDAX, UV-Vis and XRD. The photovoltaic performance of the mixed cation perovskite shows a large increase in device stability from days to weeks. The initial efficiency of mixed $Cs_xMA_{1-x}PbI_3$ devices decreases slightly, which is compensated by stability after a few days.

# 1 Introduction

The recent surge in the field of $ABX_3$-type hybrid inorganic-organic perovskite solar cells has led to a rise of efficiencies from 3.8 % in 2009 to currently 22.1 %.[1, 2, 3, 4, 5, 6, 7, 8, 9, 10] Numerous adjustments were made to the initial structure $MAPbI_3$ (MA = methylammonium $CH_3NH_3^+$) in order to obtain a more stable, non-toxic and efficient solar cell material.[11, 12, 13, 14, 15] Current record-cells usually employ a mixture of different cations and halides, as in $FA_xMA_{1-x}PbBr_yI_{3-y}$ (FA = formamidinium $(CH_3)_2NH^+$).[16, 17, 18] In fact, the plain $MAPbI_3$ has up to now failed to reach efficiencies exceeding 20 %, a benchmark that its derivatives reached in 2014.[10] This shows the importance of a judicial exploration of structural derivatives and a thorough analysis of their properties.

Halide derivatives of the plain $MAPbX_3$ span a broad compositional range $X = \{I \cdots Br \cdots Cl\}$ and allow for a continuous adjustment of the bandgap from around 1.56 eV to 3.06 eV, as lighter halides are introduced into the structure.[11, 19, 20, 21] This adjustment comes along with an increasing stability but also moves the bandgap into an unfavourable high energy region, that reduces the light harvesting range of the solar cell.[11] Furthermore the use of mixed halides is put into question because many Br-I compositions segregate upon light exposure,[22] possibly caused by thermodynamic instability of the alloy.[23]

On the other hand, A-site cation derivatives of $ABX_3$ perovskites show various enhancements. The $FAPbI_3$ perovskite has a more favourable red-shifted bandgap and is less prone to thermal degradation compared to its MA equivalent.[24] However, its photoactive $\alpha$-phase is only stable at elevated temperature and it tends to transform into the inactive $\delta$-phase at room temperature. More recently, the inorganic caesium lead halide perovskite $CsPbI_3$ has drawn a lot of attention.[25, 26, 12, 27, 28, 29, 30, 31, 32] These materials show great potential, considering that a main reason for the decomposition of perovskites is the high volatility of the organic $MA^+$ cation.[33] Cs salts are less volatile than their organic counterparts, which renders the material stable at high temperatures and can yield perovskite solar cells with an impressive thermal stability.[34, 35] However, $CsPbI_3$ also suffers from poor structural stability of its $\alpha$-phase, and tends to transform into the non-perovskite yellow $\delta$-phase at room temperature.[25] Several attempts have been made to stabilise the $\alpha$-$CsPbI_3$ with different additives.[26, 18, 32] The only long-term conservation of the dark phase at room temperature was done by co-depositing colloidal nanocrystals, that were sintered to obtain a supersaturation of $Cl^-$ dopant.[36]

Clearly, the options for plain ternary perovskite materials are limited and even more so within the range of properties that are desirable for photovoltaic applications. Therefore it seems important to further investigate mixed perovskite materials.

A substitution of the halide in the $CsPbX_3$ perovskite can be done for the halide series $X = \{I \cdots Br \cdots Cl\}$, just as in their MA derivatives.[27, 28] Besides continuous tunability in color, $CsPbI_3$ materials are viable candidates for

applications in tandem cells and exhibit an improved thermal stability.[29, 30] But just as for $MAPbX_3$ compounds, usage of lighter halide derivatives shift the bandgap into an unfavourable spectral region. Mixtures of $Cs_xFA_{1-x}PbX_3$ have been shown to maintain a desirable absorption onset and stabilise the photoactive $\alpha$-phase due to a gain in mixing entropy.[18] This improves their resistance against photo- and moisture-induced degradation.[31, 12, 32] On the other hand, mixtures of $Cs^+$ with the MA cation as in $Cs_xMA_{1-x}PbX_3$ seem to be underexplored with only one report by *Choi et al.*, which shows an improved efficiency from 5.5 to 7.7 % for a Cs-doping concentration of 10 mol%.[37] Interestingly, the more complicated ternary cation mixture $Cs_x(FA_{0.87}MA_{0.13})_{1-x}PbBr_{0.17}I_{0.87}$ was recently investigated by *Saliba et al.* and cells reached efficiencies of $> 20$ % with an impressive improvement of stability under operating conditions.[38] In this study we want to shed further light onto the seemingly under-explored $Cs_xMA_{1-x}PbX_3$ system by refining the material's compositional space and demonstrating its benefits for photovoltaic applications.

# 2 Experimental

## 2.1 Fabrication of $MAPbI_3$, $CsPbI_3$ and $FAPbI_3$ cells and cation doping

**Substrate preparation:** FTO on glass substrates of the size $7.1 \times 7.1$ cm$^2$ were cleaned by rinsing with *Decon* solution, dionised water, ethanol and then etched in an argon plasma. A 100 nm layer of $TiO_2$ was coated onto on top via spray pyrolysis. A mp$-TiO_2$ layer was deposited from a 1:10 diluted titania paste (18NR-T, Dyesol) in ethanol via spin-coating at 5000 rpm and sintering at 500 ° for 30 min, resulting in a 250 nm thick layer.

**Cation exchange:** A solution of 460 mg/mL $PbI_2$ and 23 mg/mL $PbCl_2$ in DMSO was deposited by spin-coating at 4000 rpm and annealed at 100 °C for 60 min. Dipping the lead halide film into a solution of MAI in 2-propanol (IPA) (32 mg/mL) for 2 min converted the film into the $MAPbI_3$ perovskite. The films were then washed in an IPA bath and annealed with MAI vapor at 140 °C for 60 min according to our previous report.[39] To sublime the excess MAI, we then annealed the cells for another 60min on the hotplate. For the $Cs^+$ cation exchange, we prepared a saturated solution of CsI in IPA by heating a saturated mixture with excess salt and sonicating it for 60 min. We heated the solution to 80 °C for 30 min and let it cool down to 30 °C. We then dipped the substrate into the supersaturated solution with a home-made dip coater. The substrate was partially lifted out of the CsI solution at conversion times of 1, 3, 10, 25 and 40 min in order to get different conversion stages. The film was annealed at 100 °C for 10 min. Thin-film subtrates were directly used for elemental analysis. The substrates for solar cells were covered with a solution of Spiro-MeOTAD (72 mg/mL in chlorobenzene) doped with 34 $\mu$L Li-bis-(Trifluoromethylsulfonyl)imide (540 mg/mL in acetonitrile) and 58 $\mu$L

4-tert-Butylpyridine (80 mM) and spin coating at 4000 rpm for 30 s. The cells were kept in a dry atmosphere overnight to oxygen-dope the spiro layer. Finally, a 100 nm layer of Ag was thermally evaporated as a back electrode. For the anodic contact the perovskite was scratched off the edges of the substrate and the contact was strengthened with sonication soldering. The solar cell fabrication procedure is identical to our previous report, except the cation exchange.[39]

**One-step deposition:** Equimolar precursor solutions of $MAI_{/}PbI_2$ and $CsI_{/}PbI_2$ were dissolved in DMSO with a concentration of 1 mol/L, by stirring at 60 °C over 6 h. The mixed cation solutions were prepared by mixing the $CsPbI_3$ and $MAPbI_3$ precursor solutions with the respective ratios $x = \{0.05, 0.1, 0.15, 0.2, 0.25, 0.3, 0.4, 0.5, 0.75\}$. Solutions were spin-coated at 2000 rpm for 60 s and then annealed at 100 ° for 10 min.

**Analysis:** IV performance was measured with a home-build automated scanner, using a Keithley 2400 source measurement unit. Absorption measurements were recorded with a CARY UV-Vis-NIR spectrophotometer. X-ray diffraction (XRD) measurements were performed on a Bruker D8 advanced X-ray diffractometer. All diffractograms were corrected against FTO as an internal standard.

# 3 Results and Discussion

The first step for the $MAPbI_3$ A-site cation exchange with $Cs^+$ was to find a solvent that dissolved the CsI salt without decomposing the $MAPbI_3$ perovskite. We screened several anti-solvents that are commonly used for $MAPbI_3$, but none of them showed a solubility that came close to the commonly used concentrations for cation exchanges (e.g. around 10 mg/mL or 63 mmol/L for MAI). Therefore, the sample was dipped into a supersaturated solution of CsI in IPA (that has a low solubility of CsI) for the conversion. We would like to specify that in this study we used a mixed halide precursor solution of $PbI_2$ and $PbCl_2$. However, we are using the nomenclature $MAPbI_3$ and $Cs_xMA_{1-x}PbI_3$ to refer to all species made from iodide-chloride mixed halide precursors, for the sake of simplicity. Nevertheless, the Cl does play a critical role during film formation,[40, 41, 42, 43] and has recently been shown to stabilise the photoactive $\alpha$-phase of the Cs-perovskite.[36] The organic cation exchange was done by dipping the $MAPbI_3$ films into a CsI solution in discreet steps at conversion times of 1, 3, 10, 25 and 40 min, resulting in a partially converted thin-film. We then analysed the thin-film in a high-throughput fashion with UV-Vis, XRD, EDAX, SEM and depth-analysis techniques, as shown in fig. 1. The perovskite film showed a continuous incorporation of Cs cations with increasing dipping time. This can be seen from the EDAX line scan that increases up to a Cs ratio of $x = 0.5$ for 40 min dipping time (see fig. 2). However, this steady uptake of $Cs^+$ into the structure is opposed by a discontinuity of both structural and optical properties. We saw two distinctively different steps during the conversion process.

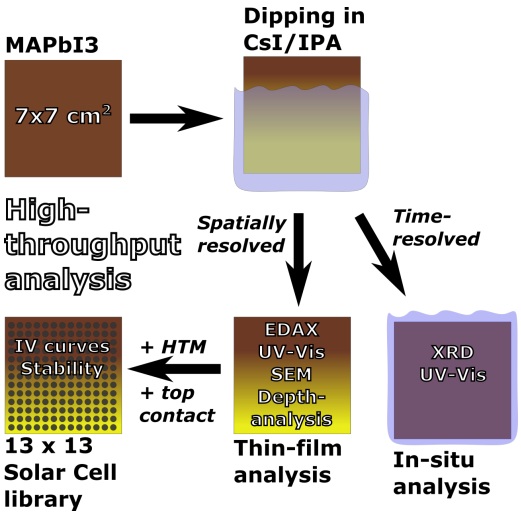


Figure 1: Schematic of the synthesis and analysis of $Cs^+$ incorporated $MAPbI_3$ cells. A gradual dipping conversion was done on $7 \times 7$ $cm^2$ substrates. The optical, electronic and structural properties of the material were tested in a high-throughput fashion. In-situ measurements were taken to clarify the conversion mechanism and show the improved stability of $Cs_xMA_{1-x}PbI_3$.

The UV-Vis analysis showed an initial blue-shift of the absorption edge (see fig. 2), caused by an increasing Cs ratio. The same trend was reported by *Choi et al.*[37] and for mixed cation systems with FA.[18, 38] Longer conversion times ($> 3$ min) resulted in a visible change of color from dark brown of the $MAPbI_3$ to a bright yellow that can be attributed to either $PbI_2$ or the $\delta$-phase of $CsPbI_3$. Accordingly, the UV-Vis spectrum showed a decrease of the $MAPbI_3$ absorption edge together with an intensifying bandgap around 440 nm. This wavelength corresponds to the signature absorption of the pure phase of $CsPbI_3$ and a indicates a discontinuity of the material, which is indicative of a miscibility gap. $PbI_2$ should show an absorption onset around 510 nm. A more detailed look shows a shifting absorption onset for initial dipping times ($\leq 3$ min) of $MAPbI_3$. This indicates incremental changes of the material, namely small inclusions of Cs before the miscibility gap. Throughout this work we labelled the incremental conversion of $MAPbI_3$ into $Cs_xMA_{1-x}PbI_3$ as *step I*, while the transformation of $Cs_xMA_{1-x}PbI_3$ into the conjugated $CsPbI_3$ caused by the miscibility gap is labelled as *step II*. In order to quantify the beginning of the miscibility gap (transition from *step I* to *step II*), we plotted the absorbance at 450 nm, as a region that is strongly absorbed by the $MAPbI_3$ and below the bandgap of *delta*-$CsPbI_3$. The absorbance shows a drop after about 3 min conversion, which correlates to a Cs ratio $x = 0.13$, as measured via EDAX.

Time-resolved analysis of the conversion was measured with in-situ XRD, as opposed to the spatially resolved analysis of the dipped films in the last section. Two distinctive regions can be seen in the measurement, that correspond to the Cs- and MA-perovskites. An excerpt that shows characteristic peaks of both perovskite domains is shown in fig. 3, while the full spectra before and after conversion are shown in the supporting information. During the course of the conversion we observed a decreasing peak intensity of the MA-containing perovskite alongside an increasing intensity of the $\delta$-phase $CsPbI_3$, indicating a

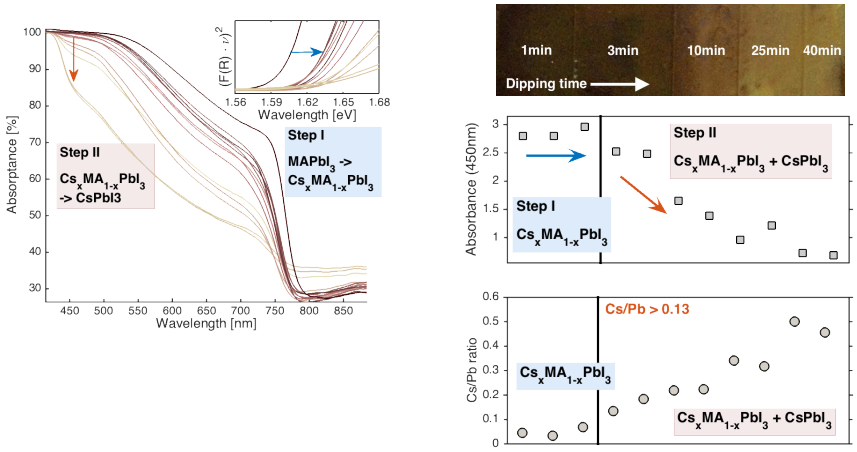


Figure 2: Absorptance spectrum (a) of $Cs^+$ intercalation into $MAPbI_3$ film for different dipping times (0−40 min). Inset (b) shows Tauc plot and bandgap shift. Optical image (c) of measured line along sample. Absorptance for wavelength 450 nm (d) along the dipping axis stays first constant and then decreases. An EDAX line scan shows a continuous increase of the Cs-ratio and correlates the drop of absorptance to a Cs ratio $x = 0.13$, indicating the formation of $\delta$-$CsPbI_3$ (full spectra in (a)).

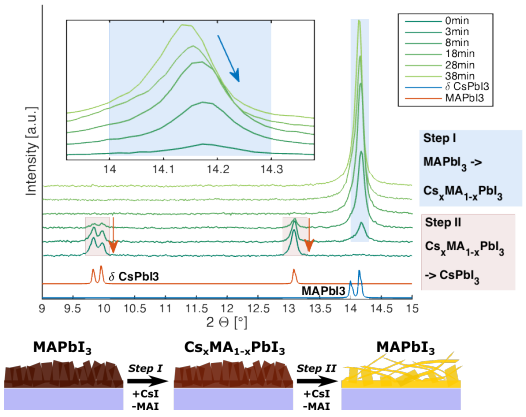


Figure 3: In-situ XRD of $Cs^+$ incorporation into $MAPbI_3$ shows two steps. First the reflection of $MAPbI_3$ shifts ([100] phase), indicating incorporation of $Cs^+$ into the 3D perovskite lattice. In the second step pure $\delta - CsPbI_3$ builds up at the expense of $Cs_xMA_{1-x}PbI_3$.

miscibility gap (*step II*) in the same fashion as discussed for the UV-Vis spectra above. Another important feature in the X-ray diffractogram is a shift of the MA-perovskite signal towards larger angles, indicating a decrease of the unit cell size. This is an effect of adding of small amounts of $Cs^+$ into the perovskite structure, as mentioned before for the *step I* formation of $Cs_xMA_{1-x}PbI_3$. The same trend is observed for $Cs^+$ incorporations into $FAPbI_3$ perovskites.[44] This shows that the miscibility gap, despite spanning a broad region, allows for small incorporations of Cs cations. A quantative discussion of this finding will be given later in this text. An out of plane movement of the focal plane caused by a layer-by-layer conversion can be excluded because the resulting shift would be beyong the detection limit. A blank measurement with IPA and without CsI salt has also been run, which showed a constant peak position.

The only comparable study on the system $Cs_xMA_{1-x}PbI_3$ was done by *Choi et al.* in 2014, as mentioned earlier, for the full compositional range of $Cs_xMA_{1-x}PbI_3$ of one-step deposited perovskites.[37] In contrast to this work, the study does not consider any phase segregation or miscibility gap. Therefore, we conducted analogous measurements on one-step deposited films of the mixed perovskite $Cs_xMA_{1-x}PbI_3$ in order to address this discrepancy and to ascertain that the miscibility gap is an intrinsic thermodynamic feature, rather than a kinetic product. The one-step deposited films all crystallised in their dark phase in the the first place. The pure $CsPbI_3$ changed its color to yellow after a few seconds on the hotplate, indicating the transition of the $\alpha$-phase into the $\delta$-phase.[26] Perovskites with Cs-contents of 75 % and 50 % endured several hours and days, respectively, before changing their color to yellow. This indicates that $MA^+$ cations can stabilise the $\alpha$-phase for a limited time, as has been reported for several other additives before.[26, 18, 36] UV-Vis analysis of the $CsPbI_3$ shows the distinct absorption onset around 450 nm, which remains conspicuous for decreasing Cs ratios down to $x \geq 0.25$. The absorption onset does not show any apparent change in wavelength (see fig. 4). On the other hand, the

bandgap of MA-rich $Cs_xMA_{1-x}PbI_3$ compounds blue-shifts continuously, from around 780 nm (1.59 eV) for $MAPbI_3$ to about 770 nm (1.61 eV), as shown in the Tauc plot (see fig. 4). Materials with a high Cs content also show an absorption onset around 510 nm, presumably relating to $PbI_2$ as a decomposition product during phase segregation. Structural analysis with XRD illustrates how the [110] diffraction peak of the $MAPbI_3$ phase decreases in intensity and shifts towards larger angles as a result of Cs-inclusion. This shift is linear for Cs-ratios $x \geq 0.15$ with a slope of 0.4012 ° (see fig. 4), which is used later to determine the Cs ratio after various dipping times as a comparison to EDAX. Larger amounts of Cs result in a peak position swinging around 14.2 °, corresponding to Cs ratios between $x = 0.1$ and $x = 0.15$. A peculiarity is the diffraction peak at 20 °, which soars for Cs ratios $x = 0.4 - 0.5$, presumably relating to the [110] side of the cubic $\alpha$-$CsPbI_3$ structure. This suggests a stabilisation of the $\alpha$-phase, that has been demonstrated before for different additives.[26, 18, 36] However, the [110] diffraction peak, and all other significant peaks of that phase, coincide with the tetragonal $MAPbI_3$ diffraction pattern facilitates a definite conclusion. For Cs-ratios $x \geq 0.25$ we can see characteristic peaks of the $\delta$-$CsPbI_3$ alongside the mixed phase $Cs_xMA_{1-x}PbI_3$. Interestingly the peak positions of the $\delta$-$CsPbI_3$ from Cs-rich mixed cation precursors ($x \geq 0.25$) are slightly shifted with respect to its pure phase, which could indicate a small solubility of $MA^+$ in the $\delta$-$CsPbI_3$. In conclusion, both synthesis routes, the one-step crystallisation and two-step conversion show continuous structural and optical changes for small inclusion of Cs and a segregation of $\delta$-$CsPbI_3$ alongside $Cs_xMA_{1-x}PbI_3$ for larger Cs ratios. This indicates that the miscibility gap is an intrinsic feature rather than a kinetic effect during the cation exchange. A similar effect of spinodal decomposition has recently been shown for halide mixtures $MAPbBr_xI_{1-x}$, caused by a broad miscibility gap.[23]

In order to investigate the depth-profile of the conversion process we exfoliated (peeled) the thin-films with adhesive tape over 15 cycles. Profilometer measurements showed that the exfoliation removed a layer with a thickness of $60 - 70$ nm in total, indicating a partial removal of the capping layer. We measured the optical absorption after each exfoliation for 15 cycles. The full absorption spectra show a decrease in absorption with each exfoliation cycle and can be found in the supporting information. Most interesting though are changes around the bandgap region, which are sensitive to small changes in the spectrum, like the bandgap shift with increasing Cs ratio shown earlier (see fig. 2). Therefore, we subtracted the spectrum of the initial (unpeeled) spectrum from the peeled sample for different time regimes of the dipping ($Abs_{peeled} - Abs_{initial}$). We can see two types of features in the subtracted spectra: (1) plateau-like regions which are caused by changes in absorbance because we take away material and (2) peaks that are caused by a shifted absorption onset between native and exfoliated thin-film. We corrected the baseline in order to have a direct comparison of the latter. The resulting spectra are shown in fig. 5. The negative peaks in the bandgap regime of $MAPbI_3$ (760 nm) demonstrate a MA-enrichement in the exfoliated capping layer, because we subtracted the initial spectrum from the peeled spectrum. Those can be seen only for short dipping times $< 10$ min and

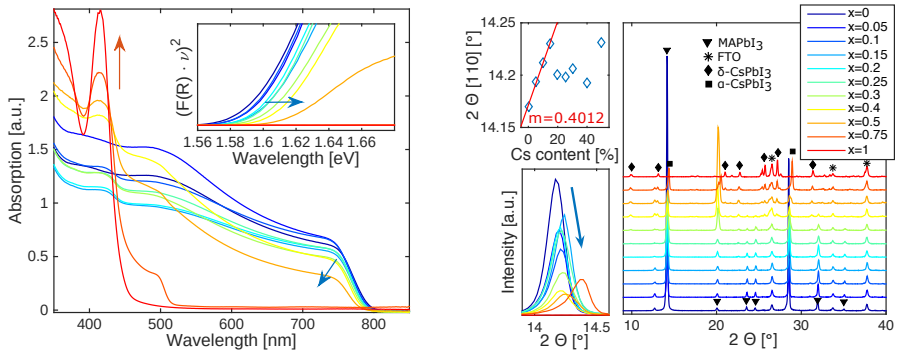


Figure 4: One-step deposited mixtures $Cs_xMA_{1-x}PbI_3$ show (a) build up of the absorption onset of $\delta$-$CsPbI_3$ for high Cs ratios x as well as a shifting bandgap for small Cs incorporations, that can also be seen in the Tauc plot (b). (c) X-ray diffractogram shows pure $MAPbI_3$ and $CsPbI_3$ at the top and bottom with their respective mixtures in between. (d) The fitted [110] diffraction peak shift continuously for Cs ratios $0 \geq x \geq 0.15$ (inset). (e) Shows a close up of the $MAPbI_3$ phase [110] peak (intensity of $x = 0$ reduced for the sake of clarity).

shows that the peeled region is MA-enriched, which indicates a faster cation exchange in the unpeeled region. This negative peak also shows a blue-shift which affirms the presence of an alloy $Cs_xMA_{1-x}PbI_3$ for small x. Spectra of films formed at longer dipping times $\geq$ 10 min do not exhibit this peak any more, which indicates Cs-saturation of the $Cs_xMA_{1-x}PbI_3$ phase. Instead, two peaks ascend at around 510 nm and 440 nm, allocated to $PbI_2$ and $\delta$-$CsPbI_3$, respectively. Vice versa, their positve signature indicates an enrichement of those species in the layer that is left after exfoliation. The position of the $CsPbI_3$ peak does not shift, which is an indication for the formation of a pure phase. On the other hand, the $PbI_2$ phase does show a blue-shift for increasing dipping times, which can be explained by intercalation dynamics, that occur during the conversion from the 3D perovskite to a 2D $PbI_2$ structure.[45, 46] We further would like to add that the presence of $PbI_2$ in the optical measurements stems from the sensitivity of the measurement, opposed to our XRD measurements which show only the perovskite structures $Cs_xMA_{1-x}PbI_3$ and $CsPbI_3$.

To quantify the stable window of the mixed phase $Cs_xMA_{1-x}PbI_3$ we used three different approaches. Using a Tauc plot, we extracted an absorption onset of 1.618 eV for $Cs_xMA_{1-x}PbI_3$ after the cation exchange, compared to 1.598 eV for the $MAPbI_3$ (see fig. 2). This correlates to a Cs ratio $x_{tauc} = 14.3$ % if we assume a linear bandgap shift between the pure compounds for small dopant concentrations and a $CsPbI_3$ bandgap of 1.73 eV.[25] The previously discussed thin-film analysis gives an estimate composition of $x_{EDAX} = 13.0$ % as the elemental composition (from EDAX) before the absorptance of $Cs_xMA_{1-x}PbI_3$ starts to drop as a result of the miscibility gap step II conversion (see fig. 2).

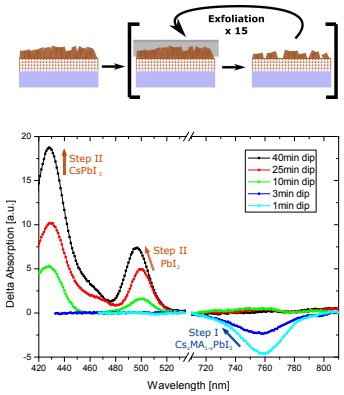


Figure 5: Depth analysis via exfoliation of the capping layer (a) shows a preferential formation of $Cs^+$ rich domains in lower sections. (b) The spectra of the difference in absorbance ($Abs_{exf}-Abs_{noexf}$, baseline removed) shows peaks in the range of the bandgaps of $Cs_xMA_{1-x}PbI_3$, $PbI_2$ and $CsPbI_3$. Negative magnitude of the $Cs_xMA_{1-x}PbI_3$ peak indicates a higher MA content in the capping layer for short dipping times ($t < 10$ min). Positive peaks for $PbI_2$ and $CsPbI_3$ indicate and enrichment in the lower mp-layer ($t \geq 10$ min).

Finally, we estimated the composition from the shifting XRD signal of the in-situ analysis of the conversion, by comparing the obtained shift with one-step deposited films with a known Cs ratio. As previously discussed, we applied a linear fit to the [110] peak position against the Cs ratio of the thin-film. The resulting slope (see fig. 4) was related to the obtained shift during cation exchange (0.048 ° after 28 min) and gave a estimated Cs ratio of $x = 11.9$ %. Combining those three methods we estimate the stable regime of $Cs_xMA_{1-x}PbI_3$ to be between $x = 0 \cdots 0.131$, as the average of our three methods, and a broad miscibility gap $x \geq 0.131$. It is worthwhile mentioning that the miscibility gap does not exist for $FAPbI_3$ compounds,[18] and can be at least partially avoided by using mixtures with formamidinium, e.g. $Cs_x(FA_{0.17}MA_{0.83})_{1-x}PbX_3$ that can achieve efficiencies $> 20$ % with an impressive stability.[38] This is somewhat surprising because the formation dynamics of perovskites can be, at least empirically, very well described by the thermochemical radii of the respective elements. The mathematical description of this correlation is given with the Goldschmidt tolerance factor $t$ and octahedral factor $\mu$.[47, 48] One might argue that the size difference between the Cs cation and MA is too large with 1.81 Å and 2.7 Å as cation radii, respectively. However, the FA cation is even larger with 2.79 Å and shows a continuous miscibility with $Cs^+$ as a perovskite.[12, 32] This points towards bonding effects that go beyond the radii of the respective $ABX_3$ ions and shows the delicacy of this class of perovskite. Possible contributions are manifold and could include factors as mixing entropy, cation shape and polarisation as well as chemical effects like hydrogen bonding, spin-orbit coupling or orbital hybridisation.[49, 50]

The appeal of a Cs-MA cation exchange for perovskite solar cells is useful to overcome the intrinsic instability of the $MAPbI_3$ perovskite,[51] which re-

Table 1: Comparison of three different methods to estimate the start of the miscibility gap for $Cs_xMA_{1-x}PbI_3$.

| Measurement | Analysis Method | Miscibility gap |
|---|---|---|
| XRD | External standard | x = 0.119 |
| EDAX | Comparison to absorption | x = 0.130 |
| UV-Vis | Tauc plot | x = 0.143 |
| | Estimated limit (average) | x = 0.131 |

mains a major obstacle towards its commercialisation. We measured decomposition rates of the $Cs_xMA_{1-x}PbI_3$ compound in comparison to the plain $MAPbI_3$ perovskite. The respective thin-films were dipped into an IPA solution with different water concentrations between 0 and 5 vol% and in-situ UV-Vis transmission was measured. Upon decomposition, the transmission spectra show a drop in the absorbance due to $MAPbI_3$ and an increasing baseline caused by the roughness of the formed $PbI_2$, resulting in an increase in light scattering. We labelled a film as decomposed when the transmission at 450 nm drops below 80 % of its initial value. The plain $MAPbI_3$ degraded relatively quickly, within 30 min in anhydrous IPA. As we increased the water concentration in IPA the films decomposed quicker, within 5 min in a solution of 5 vol% water in IPA. The $Cs_xMA_{1-x}PbI_3$ compound showed a significant increase in stability. For water concentrations $\geq$ 2 vol% the films remained intact for about twice as long. An even better performance was found for water concentrations $\leq$ 1 vol%, where the films remained stable over the duration of the measurement (10 h) and also did not show any visible decomposition after being kept another 7 days in the same solution. We would like to point out that for the $Cs_xMA_{1-x}PbI_3$ perovskite the broad spectral absorption remains intact, as opposed to changes in the halide composition that come along with a blue-shifting bandgap.[11]

Finally we wanted to investigate the photovoltaic properties of this compound. Our $MAPbI_3$ reference cell showed a conversion efficiency of $12.1 \pm 1.4$ % with the best performing cell achieving 14.2 %. For the Cs-containing sample we added a conversion step where we dipped the perovskite film into a CsI solution in IPA (details see experimental section). The photovoltage $V_{OC}$ remains persistent for all dipping times, which shows that, also for $CsPbI_3$-containing samples, the charge transport remains to be sustained through $Cs_xMA_{1-x}PbI_3$ domains. Photocurrent $I_{SC}$ showed a linear drop with dipping time, which is probably caused by the decrease in absorption (see fig. 2). The power conversion efficiency PCE also drops with increasing dipping time but the decrease in photocurrent is partially compensated by a higher fill factor FF for long dipping times. A summary of all values and averages is listed in fig. 7. We also evaluated the cell stability over a period of 31 days. Here we saw a trade-off when increasing the Cs-content: A decrease of photocurrent $I_{SC}$ is countered by a markedly improved stability. Dipping the sample for 1 min decreases the average efficiency from 12 to 10.3 % which decreases to 6.5 % after 31 days.

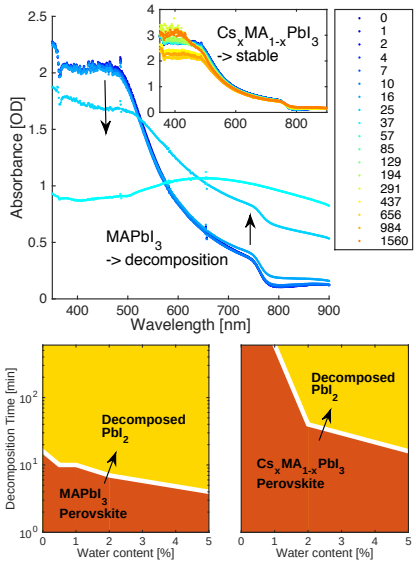


Figure 6: In-situ UV-Vis of thin-film degradation. $MAPbI_3$ and $Cs_xMA_{1-x}PbI_3$ in IPA solvent with different concentrations of water (0 – 5 vol%). $MAPbI_3$ decomposes in less than 30 min for any water concentration, while the $Cs_xMA_{1-x}PbI_3$ was stable in water concentrations $c_{H_2O} \leq 10$ wt% throughout the whole measurement (10 hours).

Dipping for 3 min gives an initial efficiency of 6.9 % that changes to 4.9 % after 31 days. In comparison, the native $MAPbI_3$ sample decreased in PCE from 12.1 % to 3.8 % in only a week. A comparison of the decomposition for the best performing native sample and the best performing $Cs^+$ dipped sample can be found in fig. 7. This shows that even short Cs conversion times have an appreciable impact on stability. Even though the initial PCE is lower for $Cs^+$ treated samples, this is been compensated by an increased stability after about 3 days, when the efficiency of the native sample drops below the mixed perovskite $Cs_xMA_{1-x}PbI_3$.

In summary, our study has investigated the incorporation of $Cs^+$ into the $MAPbI_3$ structure. Dipping the thin-film into a solution of CsI resulted in a continuous uptake of Cs cations over time. We found a maximum Cs ratio, after which the perovskite converted into the pure $\delta$-$CsPbI_3$ phase, indicating a miscibility gap. We compared this cation exchange to a one-step crystallisation procedure for different stoichiometric mixtures $Cs_xMA_{1-x}PbI_3$ and found optical and structural properties to be continuously changing for small Cs incorporations and a phase segregation for larger Cs contents. We estimate the miscibility gap of $Cs_xMA_{1-x}PbI_3$ to start at a Cs ratio $x = 0.13$, based combined measurements of EDAX, UV-Vis and XRD. We believe that these results have important implications for the fabrication of mixed cation perovskites, that are commonly employed in record cells. Furthermore, we looked at the effect of incorporations of $Cs_xMA_{1-x}PbI_3$ on stability of the material itself and in solar cells. Thin-films exposed to a mixture of water/IPA increased their stability from minutes to days. Solar cells showed an improvement in cell lifetime from days to a month, even for small incorporations of $Cs^+$ This study refines the

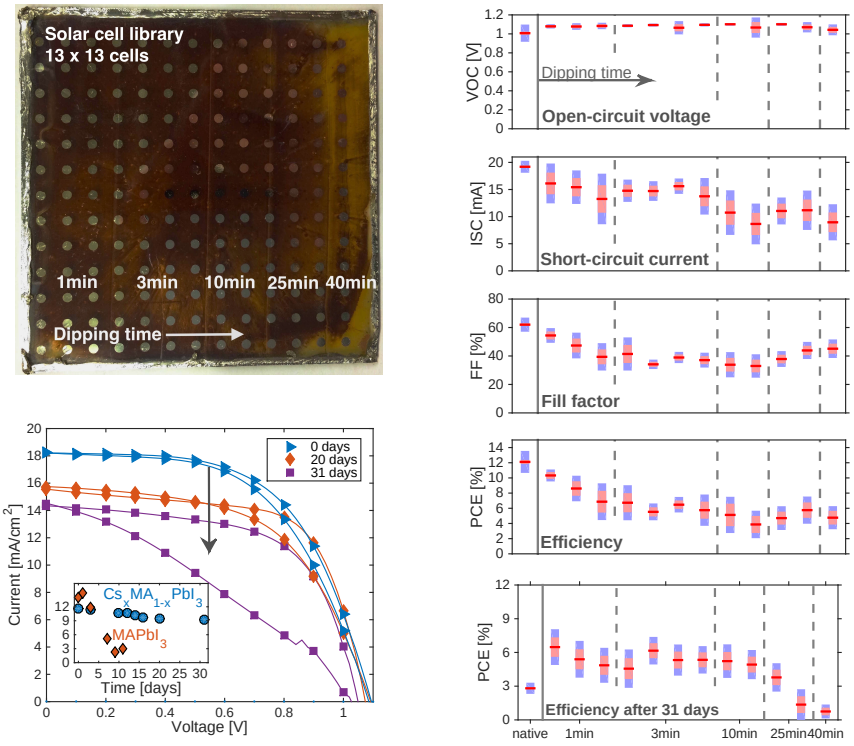


Figure 7: (a) Solar cell library (13 x 13 cells) with a gradient perovskite layer. (b) IV curves of one cell measured over 31 days. (c-f) Shows a summary of the photovoltaic parameters, namely open-circuit voltage $V_{OC}$, short-circuit current $I_{SC}$, fill factor FF and power conversion efficiency PCE, respectively. (g) PCE values after storing the library for 31 days.

compositional space and gives further manifestation to the delicacy of this class of perovskite material with implications reaching from material design to solar cell fabrication.

# References


[1] Akihiro Kojima, Kenjiro Teshima, Yasuo Shirai, and Tsutomu Miyasaka. Organometal halide perovskites as visible-light sensitizers for photovoltaic cells. *J. Am. Chem. Soc.*, 131(17):6050–1, may 2009.

[2] Jeong-Hyeok Im, Chang-Ryul Lee, Jin-Wook Lee, Sang-Won Park, and Nam-Gyu Park. 6.5% Efficient Perovskite Quantum-Dot-Sensitized Solar Cell. *Nanoscale*, 3(10):4088–93, oct 2011.

[3] Michael M Lee, Joël Teuscher, Tsutomu Miyasaka, Takurou N Murakami, and Henry J Snaith. Efficient hybrid solar cells based on meso-superstructured organometal halide perovskites. *Science (80-. ).*, 338(6107):643–647, nov 2012.

[4] Hui-Seon Kim, Chang-Ryul Lee, Jeong-Hyeok Im, Ki-Beom Lee, Thomas Moehl, Arianna Marchioro, Soo-Jin Moon, Robin Humphry-Baker, Jun-Ho Yum, Jacques E Moser, Michael Grätzel, and Nam-Gyu Park. Lead iodide perovskite sensitized all-solid-state submicron thin film mesoscopic solar cell with efficiency exceeding 9%. *Sci. Rep.*, 2:591, jan 2012.

[5] Julian Burschka, Norman Pellet, Soo-Jin Moon, Robin Humphry-Baker, Peng Gao, Mohammad K Nazeeruddin, and Michael Grätzel. Sequential deposition as a route to high-performance perovskite-sensitized solar cells. *Nature*, 499(7458):316–320, jul 2013.

[6] Mingzhen Liu, Michael B Johnston, and Henry J Snaith. Efficient planar heterojunction perovskite solar cells by vapour deposition. *Nature*, 501(7467):395–8, sep 2013.

[7] James M. Ball, Michael M. Lee, Andrew Hey, and Henry J. Snaith. Low-temperature processed meso-superstructured thin-film perovskite solar cells. *Energy Environ. Sci.*, 6(6):1739, 2013.

[8] Guichuan Xing, Nripan Mathews, Shuangyong Sun, Swee Sien Lim, Yeng Ming Lam, Michael Grätzel, Subodh Mhaisalkar, and Tze Chien Sum. Long-range balanced electron- and hole-transport lengths in organic-inorganic CH3NH3PbI3. *Science (80-. ).*, 342(6156):344–7, oct 2013.

[9] Samuel D Stranks, Giles E Eperon, Giulia Grancini, Christopher Menelaou, Marcelo J P Alcocer, Tomas Leijtens, Laura M Herz, Annamaria Petrozza, and Henry J Snaith. Electron-hole diffusion lengths exceeding 1 micrometer in an organometal trihalide perovskite absorber. *Science (80-. ).*, 342(6156):341–4, oct 2013.

[10] NREL. Research Cell Efficiency Records. \url{http://www.nrel.gov/ncpv/} [Online; accessed: 17-February-2016], 2016.

[11] Jun Hong Noh, Sang Hyuk Im, Jin Hyuck Heo, Tarak N Mandal, and Sang Il Seok. Chemical management for colorful, efficient, and stable inorganic-organic hybrid nanostructured solar cells. *Nano Lett.*, 13(4):1764–9, apr 2013.

[12] Jin-Wook Lee, Deok-Hwan Kim, Hui-Seon Kim, Seung-Woo Seo, Sung Min Cho, and Nam-Gyu Park. Formamidinium and Cesium Hybridization for Photo- and Moisture-Stable Perovskite Solar Cell. *Adv. Energy Mater.*, 5(20):1614–6840, sep 2015.

[13] Eric T. McClure, Molly R. Ball, Wolfgang Windl, and Patrick M Woodward. Cs2AgBiX6 (X = Br, Cl) New visible light absorbing, lead-free halide perovskite semiconductors. *Chem. Mater.*, 28:1348 – 1354, 2016.

[14] Adam H Slavney, Te Hu, Aaron M Lindenberg, and Hemamala I Karunadasa. A Bismuth-Halide Double Perovskite with Long Carrier Recombination Lifetime for Photovoltaic Applications. *J. Am. Chem. Soc.*, 138:2138 – 2141, feb 2016.

[15] George Volonakis, Marina R Filip, Amir Abbas Haghighirad, Nobuya Sakai, Bernard Wenger, Henry J Snaith, and Feliciano Giustino. Lead-free Halide Double Perovskites via Heterovalent Substitution of Noble Metals. *J. Phys. Chem. Lett.*, pages 1254–1259, mar 2016.

[16] Nam Joong Jeon, Jun Hong Noh, Woon Seok Yang, Young Chan Kim, Seungchan Ryu, Jangwon Seo, and Sang Il Seok. Compositional engineering of perovskite materials for high-performance solar cells. *Nature*, 517(7535):476–480, 2015.

[17] Jesper Tor Jacobsson, Juan Pablo Correa Baena, Meysam Pazoki, Michael Saliba, Kurt Schenk, Michael Grätzel, and Anders Hagfeldt. An exploration of the compositional space for mixed lead halogen perovskites for high efficiency devices. *Energy Environ. Sci.*, page In press, 2016.

[18] Chenyi Yi, Jingshan Luo, Simone Meloni, Ariadni Boziki, Negar Ashari-Astani, Carole Grätzel, Shaik M Zakeeruddin, Ursula Röthlisberger, and Michael Grätzel. Entropic stabilization of mixed A-cation ABX3 metal halide perovskites for high performance perovskite solar cells. *Energy Environ. Sci.*, 9:656–662, 2016.

[19] Yixin Zhao and Kai Zhu. Efficient Planar Perovskite Solar Cells Based on 1.8 eV Band Gap CH3NH3PbI2Br Nanosheets via Thermal Decomposition. *J. Am. Chem. Soc.*, 136(35):12241 – 44, 2014.

[20] Belen Suarez, Victoria Gonzalez-Pedro, Teresa S. Ripolles, Rafael S. Sanchez, Luis Otero, and Ivan Mora-Sero. Recombination Study of Combined Halides (Cl, Br, I) Perovskite Solar Cells. *J. Phys. Chem. Lett.*, 5(10):1628 – 35, may 2014.

[21] Ralf G. Niemann, Athanassios G Kontos, Dimitrios Palles, Efstratios I. Kamitsos, Andreas Kaltzoglou, Federico Brivio, Polycarpos Falaras, and Petra J. Cameron. Halogen Effects on Ordering and Bonding of CH3NH3+ in CH3NH3PbX3 (X = Cl, Br, I) ybrid Perovskites: A vibrational spectroscopic study. *J. Phys. Chem. C*, 120(5):2509–2519, 2016.

[22] Eric T. Hoke, Daniel J. Slotcavage, Emma R. Dohner, Andrea R. Bowring, Hemamala I. Karunadasa, and Michael D. McGehee. Reversible photo-induced trap formation in mixed-halide hybrid perovskites for photovoltaics. *Chem. Sci.*, 6:613–617, 2015.

[23] Federico Brivio, Clovis Caetano, and Aron Walsh. Thermodynamic Origin of Photoinstability in The CH3NH3Pb(I1xBrx)3 Hybrid Halide Perovskite Alloy. *J. Phys. Chem. Lett.*, 7:1083–1087, 2016.

[24] Giles E. Eperon, Samuel D. Stranks, Christopher Menelaou, Michael B. Johnston, Laura M. Herz, and Henry J. Snaith. Formamidinium lead trihalide: a broadly tunable perovskite for efficient planar heterojunction solar cells. *Energy Environ. Sci.*, 7(3):982, 2014.

[25] Constantinos C Stoumpos, Christos D Malliakas, and Mercouri G Kanatzidis. Semiconducting tin and lead iodide perovskites with organic cations: phase transitions, high mobilities, and near-infrared photoluminescent properties. *Inorg. Chem.*, 52(15):9019–38, aug 2013.

[26] Giles E. Eperon, Giuseppe M. Paterno, Rebecca J. Sutton, Andrea Zampetti, Amir Abbas Haghighirad, Franco Cacialli, and Henry J. Snaith. Inorganic caesium lead iodide perovskite solar cells. *J. Mater. Chem. A*, 3:19688–19695, 2014.

[27] Loredana Protesescu, Sergii Yakunin, Maryna I. Bodnarchuk, Franziska Krieg, Riccarda Caputo, Christopher H. Hendon, Ruo Xi Yang, Aron Walsh, and Maksym V. Kovalenko. Nanocrystals of Cesium Lead Halide Perovskites (CsPbX<inf>3</inf>, X = Cl, Br, and I): Novel Optoelectronic Materials Showing Bright Emission with Wide Color Gamut. *Nano Lett.*, 15(6):3692–3696, 2015.

[28] Quinten A. Akkerman, Valerio D'Innocenzo, Sara Accornero, Alice Scarpellini, Annamaria Petrozza, Mirko Prato, and Liberato Manna. Tuning the optical properties of cesium lead halide perovskite nanocrystals by anion exchange reactions. *J. Am. Chem. Soc.*, 137(32):10276–10281, 2015.

[29] Rachel Ellen Beal, Daniel J Slotcavage, Tomas Leijtens, Andrea Ruth Bowring, Rebecca A Belisle, William H Nguyen, George Burkhard, Eric T

Hoke, and Michael D McGehee. Cesium lead halide perovskites with improved stability for tandem solar cells. *J. Phys. Chem. Lett.*, pages 746–751, feb 2016.

[30] Rebecca J. Sutton, Giles E. Eperon, Laura Miranda, Elizabeth S. Parrott, Brett A. Kamino, Jay B. Patel, Maximilian T. Hörantner, Michael B. Johnston, Amir Abbas Haghighirad, David T. Moore, and Henry J. Snaith. Bandgap-Tunable Cesium Lead Halide Perovskites with High Thermal Stability for Efficient Solar Cells. *Adv. Energy Mater.*, page In press, jan 2016.

[31] Xiang Xia, Wenyi Wu, Hongcui Li, Bo Zheng, Yebin Xue, Jing Xu, Dawei Zhang, Chunxiao Gao, and Xizhe Liu. Spray Reaction Prepared FA1-xCsxPbI3 Solid Solution as Light Harvester for Perovskite Solar Cells with Improved Humidity Stability. *RSC Adv.*, 6:14792–14798, 2016.

[32] Zhen Li, Mengjin Yang, Ji-Sang Park, Su-Huai Wei, Joseph Berry, and Kai Zhu. Stabilizing Perovskite Structures by Tuning Tolerance Factor: Formation of Formamidinium and Cesium Lead Iodide Solid-State Alloys. *Chem. Mater.*, 28:284 – 292, 2016.

[33] Bert Conings, Jeroen Drijkoningen, Nicolas Gauquelin, Aslihan Babayigit, Jan D'Haen, Lien D'Olieslaeger, Anitha Ethirajan, Jo Verbeeck, Jean Manca, Edoardo Mosconi, Filippo De Angelis, and HansGerd Boyen. Intrinsic Thermal Instability of Methylammonium Lead Trihalide Perovskite. *Adv. Energy Mater.*, page 1500477, jun 2015.

[34] D M Trots and S V Myagkota. High-temperature structural evolution of caesium and rubidium triiodoplumbates. *J. Phys. Chem. Solids*, 69:2520–2526, 2008.

[35] Michael Kulbak, David Cahen, and Gary Hodes. How Important Is the Organic Part of the Lead Halide Perovskite Photovoltaic Cells? Efficient CsPbBr3 Cells. *J. Phys. Chem Lett.*, 6:2452 – 2456, 2015.

[36] Subham Dastidar, David A Egger, Liang Z Tan, Samuel B Cromer, Andrew DeVries Dillon, Shi Liu, Leeor Kronik, Andrew M Rappe, and Aaron T Fafarman. High Chloride Doping Levels Stabilize the Perovskite Phase of Cesium Lead Iodide. *Nano Lett.*, page In press, may 2016.

[37] Hyosung Choi, Jaeki Jeong, Hak Beom Kim, Seongbeom Kim, Bright Walker, Gi Hwan Kim, and Jin Young Kim. Cesium-doped methylammonium lead iodide perovskite light absorber for hybrid solar cells. *Nano Energy*, 7:80–85, 2014.

[38] Michael Saliba, Taisuke Matsui, Ji-Youn Seo, Konrad Domanski, Juan-Pablo Correa-Baena, Nazeeruddin Mohammad K., Shaik M Zakeeruddin, Wolfgang Tress, Antonio Abate, Anders Hagfeldt, and Michael Grätzel. Cesium-containing Triple Cation Perovskite Solar Cells: Improved Stability, Reproducibility and High Efficiency. *Energy Environ. Sci.*, page In press, 2016.

[39] Laxman Gouda, Ronen Gottesman, Shay Tirosh, Eynav Haltzi, Jiangang Hu, Adam Ginsburg, David A. Keller, Yaniv Bouhadana, and Arie Zaban. Vapor and Healing Treatment for CH3NH3PbI3-xClx Films toward Large-Area Perovskite Solar cells. *Nanoscale*, 8:6386–6392, 2016.

[40] Silvia Colella, Edoardo Mosconi, Giovanna Pellegrino, Alessandra Alberti, Valentino L P Guerra, Andrea Listorti, Aurora Rizzo, Guglielmo Guido Condorelli, Filippo De Angelis, and Giuseppe Gigli. Elusive Presence of Chloride in Mixed Halide Perovskite Solar Cells. *J. Phys. Chem. Lett.*, (5):3532 – 38, 2014.

[41] M Ibrahim Dar, Neha Arora, Peng Gao, Shahzada Ahmad, Michael Grätzel, and Mohammad Khaja Nazeeruddin. Investigation Regarding the Role of Chloride in Organic-Inorganic Halide Perovskites Obtained from Chloride Containing Precursors. *Nano Lett.*, 14(12):6991 – 96, 2014.

[42] Vanessa L. Pool, Aryeh Gold-Parker, Michael D. McGehee, and Michael F. Toney. Chlorine in PbCl2-Derived Hybrid-Perovskite Solar Absorbers. *Chem. Mater.*, 27(21):7240–7243, 2015.

[43] Chenghao Cao, Chujun Zhang, Junliang Yang, Jia Sun, Shuping Pang, Han Wu, Runsheng Wu, Yongli Gao, and Chengbin Liu. Iodine and Chlorine Element Evolution in CH3NH3PbI3-xClx Thin Films for Highly Efficient Planar Heterojunction Perovskite Solar Cells. *Chem. Mater.*, page In press, 2016.

[44] David P McMeekin, Golnaz Sadoughi, Waqaas Rehman, Giles E Eperon, Michael Saliba, Maximilian T Hörantner, Amir Haghighirad, Nobuya Sakai, Lars Korte, Bernd Rech, Michael B Johnston, Laura M Herz, and Henry J Snaith. A mixed-cation lead mixed-halide perovskite absorber for tandem solar cells. *Science (80-. ).*, 351(6269):151–155, jan 2016.

[45] N Preda, L Mihut, M Baibarac, I Baltog, and S Lefrant. A distinctive signature in the Raman and photoluminescence spectra of intercalated PbI2. *J. Phys. Condens. Matter*, 18:8899–8912, 2006.

[46] I Baltog, M Baibarac, and S Lefrant. Quantum well effect in bulk PbI(2) crystals revealed by the anisotropy of photoluminescence and Raman spectra. *J. Phys. Condens. Matter*, 21:025507, 2009.

[47] H. D. B. Jenkins and K P Thakur. Reappraisal of Thermochemical Radii for. *J. Chem. Educ.*, 56(9):576–577, 1979.

[48] Helen K Roobottom, H Donald B Jenkins, Jack Passmore, and Leslie Glasser. Thermochemical Radii of Complex Ions Estimation of Thermochemical. *J. Chem. Educ.*, 76(11):1570–1573, 1999.

[49] Feng Wang, Jiale Ma, Fangyan Xie, Linkai Li, Jian Chen, Jun Fan, and Ni Zhao. Organic Cation-Dependent Degradation Mechanism of Organotin Halide Perovskites. *Adv. Funct. Mater.*, page In press, 2016.

[50] Aron Walsh. Principles of Chemical Bonding and Band Gap Engineering in Hybrid OrganicInorganic Halide Perovskites. *J. Phys. Chem. C*, 119:5755–5760, 2015.

[51] Yue-Yu Zhang, Shiyou Chen, Peng Xu, Hongjun Xiang, Xin-Gao Gong, Aron Walsh, and Su-Huai Wei. Intrinsic Instability of the Hybrid Halide Perovskite Semiconductor CH3NH3PbI3. *arXiv Prepr.*, page arXiv:1506.01301, 2015.